



## Evolution of Strength and Permeability in Stressed Fractures with Fluid–Rock Interactions

ZHEN ZHONG,<sup>1,2</sup> DEREK ELSWORTH,<sup>3</sup> and YUNJIN HU<sup>1,2</sup>

**Abstract**—We determine the evolution of frictional strength, strain weakening behavior and permeability in fractures subject to dissolution and precipitation. We establish these relations through slide–hold–slide experiments, with hold times from 10 to 3000 s, on split limestone core, under hydraulically open and closed conditions. Fracture friction and permeability are measured continuously throughout the experiments. The limestone displays velocity-strengthening behavior (stable slip) under incremented velocity steps of 1–6  $\mu\text{m/s}$ . Frictional healing is observed to be time- and stress-dependent, showing higher gains in strength at both longer hold times and under lower effective stresses. Activation of healing is greater in wet samples than in dry samples. Flow-through experiments for flow rates in the range of 1–10 ml/min are conducted to further investigate the role of flow and mineral redistribution in contributing to healing. These experiments show strength gains are lower at higher flow rates where advective mineral dissolution and redistribution is enhanced and cementation concomitantly limited. Concurrently measured permeability decreases throughout the slide–hold–slide sequences indicating that mean fracture aperture reduces during sliding. We combine models representing pressure solution and stress corrosion as models for the growth in fracture contact area and represent the observed time-dependent behavior of strength gain and permeability evolution. The simulated results represent the observed strengthening at long hold times ( $\sim 1000$  s), but underestimate strengthening at short hold times. We conclude that the evolution of strength and permeability are significantly controlled by mechanisms of fluid–rock interactions and that the strengths and nature of feedbacks on these linkages are critical in understanding the mechanical and hydraulic behavior of faults.

**Key words:** Strength evolution, permeability evolution, frictional healing, velocity strengthening, fluid–rock interactions.

### 1. Key points

Strength and Permeability evolution are determined via a suit of experiments  
Fluid–rock interactions exert significant effects on strength and stability evolution  
A mechanistic model is applied to describe the observed frictional healing

### 2. Introduction

The evolution of the mechanical and hydraulic properties of fractures and faults exerts a critical influence on the behavior of fault zones and on the earthquake cycle. In addition to natural processes, this behavior has broad implications in induced seismicity and influences oil and gas production, the sequestration of carbon dioxide and the disposal of nuclear wastes.

Fault friction is typically measured by slide–hold–slide experiments, where fault gouge is deformed at low velocities ( $<0.1 \text{ mms}^{-1}$ ) and over small shear offsets ( $<30$  mm) (DIETERICH 1979, 1981; MAIR *et al.* 1999; MARONE 1998, 2004) or alternatively with rotary-shear devices, that enable higher slip velocities over very large shear offsets (HIROSE and SHIMAMOTO 2005; MIZOGUCHI *et al.* 2006). Typical experiments (DIETERICH 1972; MARONE 1998; OLSEN *et al.* 1998; BOS and SPIERS 2002; TENTHOREY *et al.* 2003) show significant creep during the holding period and frictional healing (strength gain) upon reloading. Fault creep and healing are often time-dependent with longer hold times typically resulting in greater magnitudes of creep and in strength gains (TENTHOREY *et al.* 2003; YASUHARA *et al.* 2005; CARPENTER *et al.* 2012). Frictional healing may arise from growth of

<sup>1</sup> College of Civil Engineering, Shaoxing University, No.508 Huancheng West Rd., Shaoxing 312000, China. E-mail: huyunjin@zju.edu.cn

<sup>2</sup> Hydraulic Engineering, Hydraulic Structure and Water Environment Institute, Zhejiang University, 866 Yuhangtang Rd., Hangzhou 310058, China.

<sup>3</sup> Energy and Mineral Engineering, EMS Energy Institute, G3 Center, Pennsylvania State University, University Park, PA 16802-5000, USA.

grain contacts (potentially induced by pressure solution) (RABINOWICZ 1951; DIETERICH and KILGORE 1994; YASUHARA *et al.* 2005), strengthening of the contacts (correlates with cementation) (HICKMAN and EVANS 1992; BEELER *et al.* 1994; KARNER *et al.* 1997; OLSEN *et al.* 1998; MUHURI *et al.* 2003; TENTHOREY *et al.* 2003; LI *et al.* 2011) or via other changes in state including changes in porosity and rearrangement of force chains (GOREN *et al.* 2010, 2011). Experimental evidence (DIETERICH 1979, 1981; JOHNSON 1981; MARONE and SCHOLZ 1988; MARONE 1998; SAFFER and MARONE 2003; MOORE and LOCKNER 2007; IKARI *et al.* 2007, 2011; CARPENTER *et al.* 2012) quantifies both the mode and magnitude of second-order changes in the velocity-dependent (including velocity-strengthening and weakening) evolution of frictional strength. Velocity strengthening results in stable slip, whereas velocity weakening may result in unstable slip.

Related to this crucial link of second-order frictional response to mineralogy, fluid–rock interactions exert an important influence on the mechanical and hydraulic behavior of faults (EVANS and CHESTER 1995; HICKMAN *et al.* 1995; RENARD *et al.* 2000; TENTHOREY *et al.* 2003; YASUHARA *et al.* 2006; GIGER *et al.* 2007; MIZOGUCHI *et al.* 2007; VIOLAY *et al.* 2013, 2014) through pressure solution, through cementation (YASUHARA *et al.* 2004, 2005, 2006; MCGUIRE *et al.* 2013) and through fabric evolution (WINTSCH *et al.* 1995; HOLDSWORTH 2004; COLLETTINI *et al.* 2009a, b; NIEMEIJER *et al.* 2010a). Pressure solution includes processes of dissolution, diffusion and precipitation (YASUHARA *et al.* 2003). Augmentation in strength (healing) has been attributed to the gain in contact area of particle intergrowths, mediated by pressure solution (YASUHARA *et al.* 2005) and additional influences on dilation that result from the behavior of bonded aggregates. The generation of wear products during sliding contact alternately results in cementation (RENARD *et al.* 2000), which may temporarily increase fault strength before returning to stable slip (RECHES and LOCKNER 2010). The relative strengths of pressure solution and cementation effects determine the ultimate healing magnitude (YASUHARA *et al.* 2005) and related change in strength but may also condition a change in permeability (MCGUIRE *et al.* 2013)—either a reduction or enhancement. Despite active research in exploring fault evolution for a wide

range of conditions, the response of fault healing and permeability evolution resulting from fluid–rock interactions (chemical–mechanical coupling) remains poorly understood.

We report slide–hold–slide and velocity-stepping experiments on split limestone cores under both dry and wet conditions. The samples are sheared at a constant velocity under a range of effective normal stresses (1, 3, and 5 MPa). The evolution of friction and of permeability are measured concurrently during the experiments—the latter using the steady flow rate of distilled water circulating through the fracture to measure the evolution in permeability. The observed frictional healing and change in permeability is interpreted through a modified mechanistic model of pressure solution (YASUHARA *et al.* 2003) applied over the contacting fracture.

### 3. Experimental approach

We complete a suite of short-term (~hours) experiments using axially split core within a standard simple triaxial cell. Experiments are conducted both dry and wet.

#### 3.1. Experimental sample

The samples used in the experiment are produced from axially split limestone core (50 mm long by 25 mm diameter). The core is saw-cut into two halves and the surfaces are roughened to a repeatable roughness using 60-grit ceramic abrasive (MCGUIRE 2012). The sample is assembled by re-mating the two halves with a 1-cm preset right-lateral offset allowing left-lateral shearing in the apparatus to null offset. The offset sample is encased in a latex jacket to allow both the application of confining (normal) stress and to enable fluid circulation along the saw-cut fracture.

#### 3.2. Experimental setup

A standard triaxial apparatus is used for the various shearing experiments. The experimental arrangement is shown in Fig. 1. The fractured sample (the fracture along the axial direction) with an initial offset of 1 cm is packed within dual latex membranes

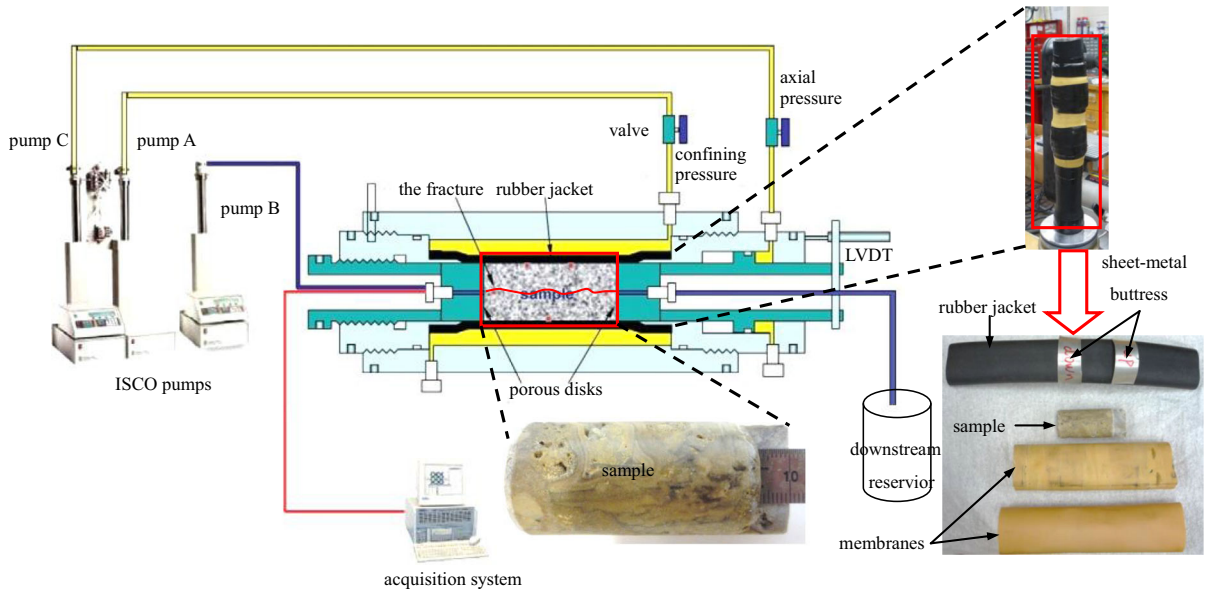


Figure 1  
Schematic of the standard triaxial apparatus and sample assembly

representing an interior and exterior seal. The diametrically opposed half-cylindrical voids at each end of the sample that result from the initial shear-offset of the fracture are protected from intrusion of the membrane by a sheet-metal arch. The packed sample is then assembled between two cylindrical stainless steel end-platens plumbed with fluid connections and the assembly placed within the triaxial core holder (Temco). Three Isco D-series syringe pumps with control to  $\pm 0.007$  MPa are used to control the stresses applied to the sample. Pumps A and C (Isco 500D) are used to apply normal and axial stresses, respectively, and pump B (Isco 100DM) is used for the injection of fluid to the inlet platen and from there along the length of the sample. Pressure and flow rate of the pumps are recorded via a (National Instruments) LabView DAQ system. Concentrations of major species (calcium and other major ions) are measured in the effluent fluid by periodic sampling and by assaying using inductively coupled plasma emission spectrometry (Perkin-Elmer Optima 5300 ICP/MS) to  $\pm 0.0001$  ppm ( $\mu\text{g/mL}$ ). Axial displacement under the applied shear stress is measured by a linear variable displacement transducer (LVDT, Trans-Tek 0244) to  $\pm 1$   $\mu\text{m}$  as a confirmation

of the displacement rate applied by the pump and the measured axial stress (pump C).

Resistance between rock and membrane is calibrated by connecting the inlet and outlet platens to pump B, whose pressure is set equal to the normal stress of pump A, so that membrane resistance can be calculated by the measured axial stress and at zero effective stress.

The equation of static equilibrium for the half core is defined as:

$$\begin{aligned} F_a &= F_M + F_S = F_E + (\sigma_n - P_c)A_c \\ &= F_M + \left( \sigma_n - \frac{P_I + P_O}{2} \right) A_c, \end{aligned} \quad (1)$$

where  $F_a$  is the axial force,  $F_M$  is the tangential force exerted by the membrane on the half-cylinder, and  $F_S$  is the frictional force between the roughened fracture surfaces.  $\sigma_n$  is the normal stress, and  $P_c$  is the pore pressure at the midpoint along the length of the sample.  $P_I$  and  $P_O$  represent the pore pressure of the flow inlet and outlet platens, respectively.  $A_c$  is the interface area between roughened fracture surfaces.

Connecting the inlet and outlet platens to pump B, whose pressure is set equal to the normal stress ( $\sigma_n$ ), results in,

$$\sigma_n = P_I = P_O = \frac{P_I + P_O}{2}. \quad (2)$$

Substituting Eq. (2) into Eq. (1) yields,

$$F_a = F_M + \left( \sigma_n - \frac{P_I + P_O}{2} \right) A_c = F_M + 0 = F_M. \quad (3)$$

The frictional data recovered from direct observations are corrected for membrane resistance effects.

### 3.3. Experimental procedure

We performed slide–hold–slide (SHS) and velocity-stepping (VS) tests on dry samples placed in the cell at ambient humidity. The SHS tests were conducted at invariant effective normal stresses of 1 MPa, incremented to 3 MPa and then 5 MPa after steady-state friction was attained. The sample was sheared at a constant velocity of 3  $\mu\text{m/s}$  during the slide sequence. Hold times range from 10 to 3000 s. Both dry and wet samples were used in the SHS tests to account for the influence of water on frictional healing and creep. In the flowing experiments on saturated samples, a range of flow rates (1, 3, 5, and 10 ml/min) was used to further explore the influence of fluid circulation on the evolution of permeability with strength. The VS experiments were conducted for various shear velocities at 3 MPa effective normal stress to follow the evolution of frictional stability and in particular velocity-weakening/strengthening effects. Permeability was measured continuously throughout the shearing experiments under conditions of incremented effective normal stress steps at 1, 1.5, 2, and 3 MPa and at a constant shearing velocity of 1  $\mu\text{m/s}$ . Upstream reservoir pressure was maintained at 0.1 MPa with the downstream reservoir at atmospheric pressure (0 MPa gauge).

## 4. Observations and Discussion

The evolution of frictional strength was measured using SHS experiments on first dry and then wet samples to define the role of water as a solvent in influencing healing and creep behavior of reactive media (limestone). These are conducted under both

hydraulically closed and open conditions with concurrent measurement of permeability evolution and of redistribution of mineral mass within the shearing fracture. These observations are supplemented by measurements of the evolution of second-order frictional stability using velocity-stepping (VS) experiments. Observations from these experiments are compared against models for mineral redistribution and the evolution of frictional behavior, constrained by experimental measurements.

### 4.1. Observations

SHS experiments were first conducted on a dry sample under effective normal stresses of 1, 3, and 5 MPa and with hold times of 10–3000 s. The experiment was then paused, the sample saturated with deionized (DI) water and SHS experiments resumed with circulation of DI water at the low relative flow rate of 1 ml/min. The evolution of interface friction, on both dry and wet samples under a variety of effective normal stresses is shown in Fig. 2. Frictional healing and creep are both apparent in the SHS experiments (see inset of Fig. 2a) together with their dependency on hold time and ambient stresses. Both frictional healing and frictional creep increase with an increase in hold time, but decrease with an increase in normal stress (Fig. 2b, c). Both frictional healing and creep are enhanced when the sample is saturated and then flushed with water with the wet sample exhibiting greater healing and creep than the dry sample.

The evolution of frictional healing and creep were then examined for water-saturated samples where flow-rate is incremented from 1 to 10 ml/min (Fig. 3). Apparent from these observations are that magnitudes of frictional healing and creep both decrease with an increase in flow rate. This may result from the removal of wear products as a result of increased dissolution and advective removal of mineral mass or by limiting the opportunity for cementation to progress by a similar mechanism—advective mineral redistribution and removal.

Velocity-stepping (VS) experiments were conducted under a constant effective normal stress of 3 MPa. The steady coefficient of friction increases with an increase in shear velocity (Fig. 4). These

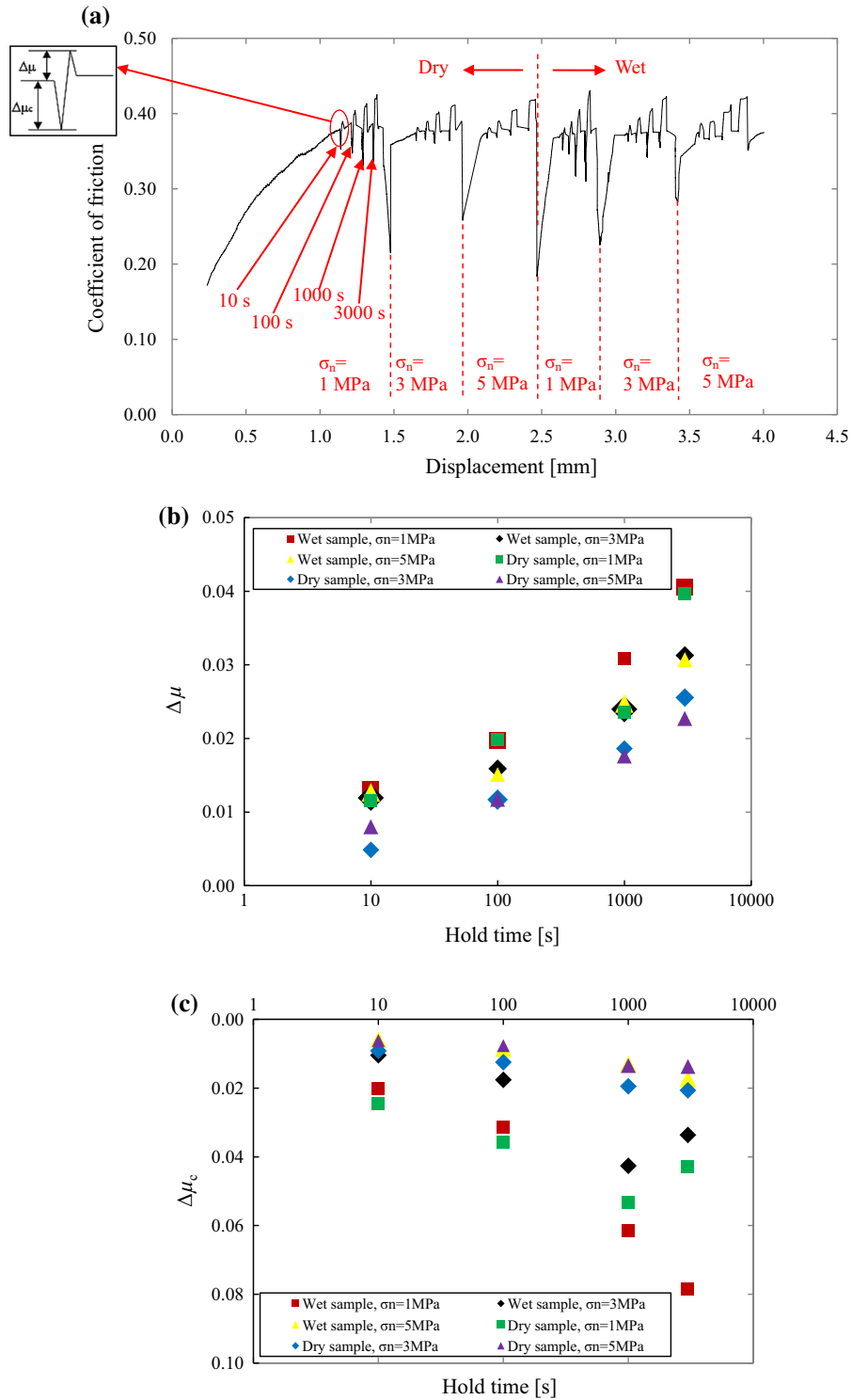


Figure 2

Results of SHS tests for both dry and wet samples under 1, 3, 5 MPa effective normal stresses. Corrected ratios of shear stress to effective normal stress (coefficient of friction) as a function of displacement at a shearing velocity of  $3 \mu\text{m/s}$  (a). Time history of evolution of friction coefficient  $\mu$ . b SHS-derived frictional healing increment  $\Delta\mu$ , and c frictional creep increment  $\Delta\mu_c$ .

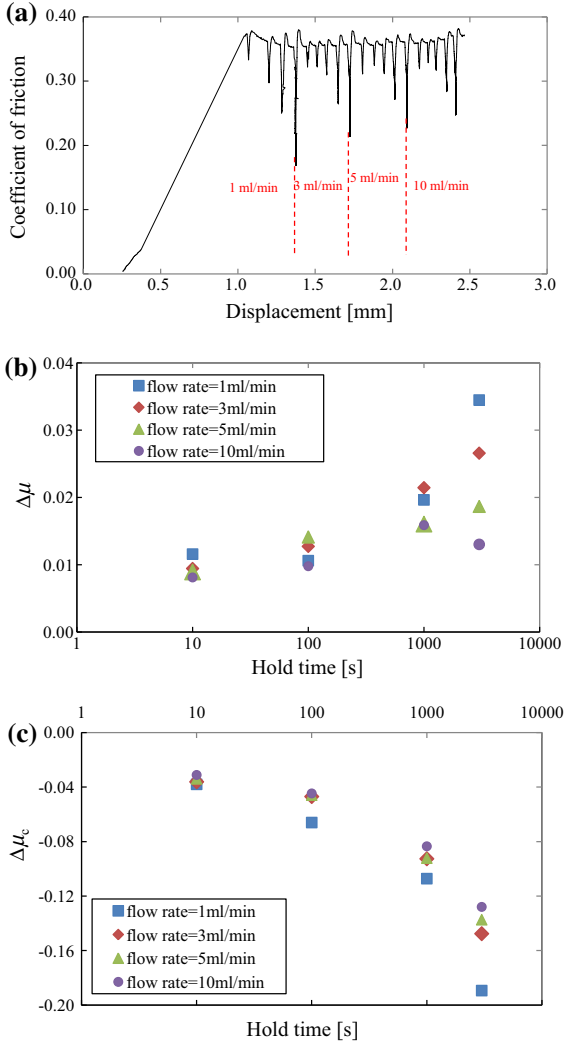


Figure 3

Frictional evolution in flow-through experiments on water-saturated samples under 1 MPa effective normal stress. Corrected data of strength evolution at flow-rate incremented from 1 to 10 ml/min (a). Time history of evolution of friction coefficient  $\mu$ . b SHS-derived frictional healing increment  $\Delta\mu$ , and c frictional creep increment  $\Delta\mu_c$ .

results indicate that the split limestone core displays uniform velocity-strengthening behavior. This is compatible with recent observations showing velocity strengthening in limestone at low temperatures (25–50 °C) (VERBERNE *et al.* 2010).

Frictional stability is quantified by the friction rate parameter  $a - b$ ; defined as

$$a - b = \frac{\Delta\mu_{ss}}{\ln(V/V_0)}, \quad (4)$$

where  $a$  and  $b$  are empirically derived constants (unitless) and  $\mu_{ss}$  describes the change in the steady-state coefficient of friction upon an increase in sliding velocity from  $V_0$ – $V$  (MARONE, 1998).

We calculated  $a$ ,  $b$  and  $a - b$  upon sliding velocity increasing from 1.5 to 3  $\mu\text{m/s}$ : the  $a - b$  value is positive, indicating inherently stable sliding (SCHOLZ 1998). The  $b$  value is negative, which has been reported previously for various minerals at elevated temperature (IKARI *et al.* 2009; NIEMEIJER and VISSERS 2014, and reference therein). Negative  $b$  value may occur when the contact lifetime is sufficiently small (IKARI *et al.* 2009).

Figure 5 shows the evolution of permeability at four effective normal stresses (1, 1.5, 2, 3 MPa). Permeability decreases as the normal stress is incremented and also near monotonically with shear displacement—suggesting that either the fracture is compacting or that wear products begin to dominate the permeability response. We discuss these mechanisms later.

#### 4.2. Discussion

We attempt to reconcile the various observations for the evolution of first- and second-order frictional behavior and transport properties with a mechanistic understanding. The observation that healing rates and creep rates both increase with an increase in hold time (Fig. 2) is consistent with mechanisms of growing surface area or by cementation as a result of increased chemical activity by pressure solution or by stress corrosion (YASUHARA and ELSWORTH 2008). A decrease in healing and creep relaxation with an increase in normal stress (Fig. 2) is partly congruent with growth of cementation—as the contribution of adhesion that results from cementation will become progressively less important as shear strength builds by higher friction at higher normal stresses. Finally, the observation that strength gains due to healing and creep both grow with a reduction in flow rate (Fig. 3) and the concomitant reduction in the removal of potential cements from the asperity contacts is also congruent with an anticipated increase in cementation or growth in contact area.

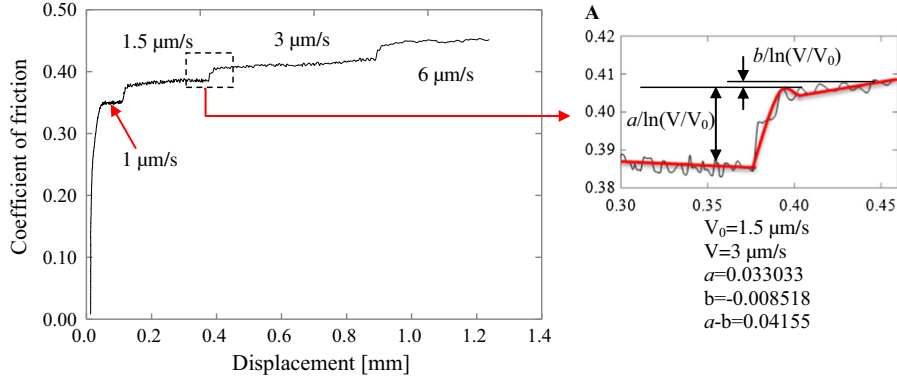


Figure 4

Corrected results of velocity-stepping (VS) experiments. Evolution of friction at a constant normal stress of 3 MPa, with shearing velocities ranging from 1 to 6  $\mu\text{m/s}$ . Inset a inset is of velocity steps shifting from 1.5 to 3  $\mu\text{m/s}$

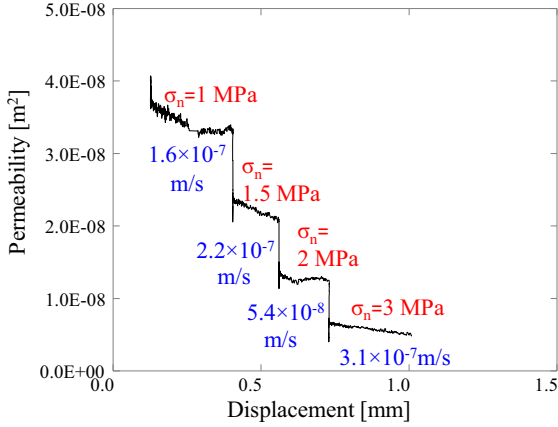


Figure 5

Measured permeability (black line) versus shear displacement for effective normal stresses of 1, 1.5, 2 and 3 MPa with rates of change of fracture aperture (blue) recovered from permeability magnitudes. Aperture change rates are used to constrain mineral redistribution (dissolution versus precipitation) within the sample and to constrain principal active processes

These observations suggest that cementation or growth in contact areas is a consistent mechanism to support these observations. However, further constraints may be placed on this by the concurrent measurements for the evolution of transport properties. The fracture is the major conduit of fluid flow for the ambient low-permeability matrix (VOLERY *et al.* 2010). Thus the discharge ( $Q$ ) can be shown in the form of Darcy's law as

$$Q = \frac{k}{\mu} A \frac{(P_{\text{up}} - P_{\text{down}})}{L} = \frac{k \pi D^2}{\mu 4} \frac{(P_{\text{up}} - P_{\text{down}})}{L}, \quad (5)$$

where  $k$  is the equivalent porous-medium-measured permeability,  $\mu$  is the dynamic viscosity,  $A$  is the

cross-sectional area of the sample,  $D$  and  $L$  are the diameter and length of the sample, respectively, and  $P_{\text{up}}$  and  $P_{\text{down}}$  represent the upstream and downstream pressure, respectively. When the actual flow is along a fracture of aperture  $b$ , then

$$Q = \frac{D b^3 (P_{\text{up}} - P_{\text{down}})}{\mu 12 L}. \quad (6)$$

Substituting Eq. (6) into Eq. (5) enables fracture aperture ( $b$ ) to be determined from the flow-rate and equivalent porous medium permeability for the sample as

$$b = \sqrt[3]{3\pi k D}. \quad (7)$$

Thus rates of change of the fracture aperture ( $db/dt$ ) may be recovered from the SHS experiments. As shown in Fig. 5, the reduction in permeability correlates with a reduction in aperture—if the influence on permeability is assumed to result solely from fracture closure. If the generation of significant quantities of wear products are implicated in this change in permeability, then a different model is required to represent the response. We attempt to link such causal mechanisms contributing to growth in contact area or cementation to the evolution of transport behavior. Reduction in permeability with an increase in normal stress (Fig. 5) is likely due to elastic closure of the fracture. The monotonic reduction in fracture permeability with shear (Fig. 5) is likely due to the dominant impact of the generation of wear products over fracture dilation as normal

stresses increase and shear dilation is suppressed (Fig. 5).

Mechanical and hydraulic response of faults are controlled by combined processes of stress corrosion (ATKINSON 1979; CHESTER *et al.* 2004; NARA and KANEKO 2005), pressure solution (ROBIN 1978; DEWERS and HAJASH 1995; REVIL 1999; YASUHARA *et al.* 2004) and cementation (HICKMAN and EVANS 1992; KARNER *et al.* 1997; OLSEN *et al.* 1998; BOS *et al.* 2000; BOS and SPIERS 2002; MUHURI *et al.* 2003; TENTHOREY *et al.* 2003; MCGUIRE 2012). The first two processes are driven by the local or intergranular effective normal stress and all processes are mediated by the hydraulic conditions of the fault including flow-rate and aqueous concentrations of pore fluids. The effluent calcium concentration is measured in order to understand the role of stress in driving these behaviors. Congruent with prior studies (SCHOLZ 2002; MUHURI *et al.* 2003; TENTHOREY *et al.* 2003; YASUHARA *et al.* 2005), frictional healing during SHS experiments shows an approximately linear relation with the log of hold time (see Fig. 6). From these observations, we constrain response using models that represent key mechanisms of cementation using the growth in contact area as a proxy.

We use a mechanistic model (including a series of processes of pressure solution, free face dissolution and precipitation to the pore wall) for the progress of

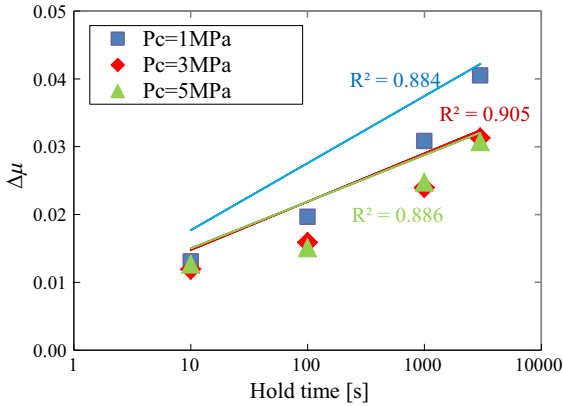


Figure 6

Frictional healing [see inset (b) of Fig. 2] with hold time for SHS experiments on wet sample at effective normal stresses of 1 MPa (blue square), 3 MPa (red diamond) and 5 MPa (green triangle). The solid lines with different colors are log-linear fit of corresponding effective normal stresses,  $R^2$  is the coefficient of determination

pressure solution (YASUHARA *et al.* 2003) to follow the evolution of contact area as a proxy for healing. The mechanistic model assumes that, to first order, strength gain is proportional to the contact area growth  $[(A_c)_{ps}/A_{c0}]$  that arises from pressure solution. The predictive results, for parameters listed in Table 1, are compared with experimental results measured at the effective normal stress of 3 MPa (shown in Fig. 7). It is apparent that the model significantly underpredicts the measured frictional healing at short hold times. This under-prediction may be attributed to two reasons. First, the influence of pressure solution is smallest in this range of the parameter space (YASUHARA *et al.* 2005), i.e., under low effective stresses, and the second is that the model neglects stress corrosion and the explicit effects of cementation. To remedy this, we augment the mechanistic model by attempting to constrain and to then include the influence of stress corrosion on the resulting response.

The decrease in permeability that results during hold periods (see Fig. 5) suggests that the fracture is closing, as any contributing wear products are already in place and no new products are likely generated. We attribute this closure to either the effects of stress corrosion, which may be dominant in fracture compaction under low temperatures (YASUHARA and ELSWORTH 2008) or possibly due to pressure solution. Increments in closure during hold times can be calculated from effluent fluxes through Eq. (8), and then grain-to-grain contact area growth caused by stress corrosion is derived from Eq. (9).

The decrement in fracture aperture can be derived from Eq. (6),

$$\begin{aligned} \Delta b &= b_{\text{int}} - b_{\text{end}} \\ &= \sqrt[3]{\frac{12\mu L}{D(P_{\text{up}} - P_{\text{down}})} Q_{\text{int}}} \\ &\quad - \sqrt[3]{\frac{12\mu L}{D(P_{\text{up}} - P_{\text{down}})} Q_{\text{end}}}, \end{aligned} \quad (8)$$

where subscripts int and end denote the beginnings and then end of the hold periods, respectively.

As shown in Fig. 8, grain-to-grain contact area growth induced by stress corrosion is calculated through Eq. (9),

Table 1

<i>Material parameters utilized in the numerical model</i>		
Parameter	Value	Reference
Grain diameter $d$ , $\mu\text{m}$	14	ZHANG <i>et al.</i> (2010)
Temperature $T$ , $^{\circ}\text{C}$	25	
Mean effective stress $\sigma_{\text{eff}}$ , MPa	3.0	
Poisson ratio $\nu$	0.3	
Young's modulus $E$ , GPa	20	
Critical stress $\sigma_c$ , MPa	60.3	
Diffusion path thickness $\omega$ , nm	4.0	YASUHARA <i>et al.</i> (2005)
Diffusion coefficient $D_b$ , $\text{m}^2\text{s}^{-1}$	$1.0 \times 10^{-10}$	NAKASHIMA (1995)
Dissolution rate constant $k_+$ , $\text{mol m}^{-2}\text{s}^{-1}$	$1.63 \times 10^{-6}$	CUBILLAS <i>et al.</i> (2005)
Precipitation rate constant $k_-$ , $\text{mol m}^{-2}\text{s}^{-1}$	$1.0 \times 10^{-6.41}$	INSKEEP and BLOOM (1985)
Solubility of calcite $C_{\text{eq}}$ , ppm	20	GRATIER <i>et al.</i> (2013)

$$(A_c)_{sc} = \pi \left( \frac{(d_c)_{sc}}{2} \right)^2 = \pi \left( \left( \frac{d}{2} \right)^2 - \left( \frac{d}{2} - \Delta b \right)^2 \right), \quad (9)$$

where  $(d_c)_{sc}$  is the diameter of contact,  $d$  is the diameter of the grain.

The total contact area growth consists of growths caused jointly by pressure solution and stress corrosion as:

$$A_c = (A_c)_{ps} + (A_c)_{sc}, \quad (10)$$

where  $(A_c)_{ps}$  is grain-to-grain contact area growth motivated by pressure solution (YASUHARA *et al.* 2003).

The total growth of contact area uses a 10-fold dissolution/precipitation rate constant ( $k_+/k_-$ ) as shown in Fig. 7 (solid line). The early predictions (solid line) still underestimate the experimental observation, but the subsequent estimations ( $>1000$  s) represent the observed strength gain reasonably well.

## 5. Conclusions

Laboratory experiments have been performed to evaluate the strength and permeability evolution of split limestone cores under fluid-rock interactions. SHS tests show that frictional strength exhibits significant healing and creep, which is both time- and stress-dependent. Frictional healing and creep are also influenced by fluid-rock interactions. Wet samples, activated by water, display a slightly greater healing rate and creep rate than dry samples. This healing rate is somewhat constrained as the flow rate increases—an increase in flow rate causes a decrease in healing rate. We invoke a

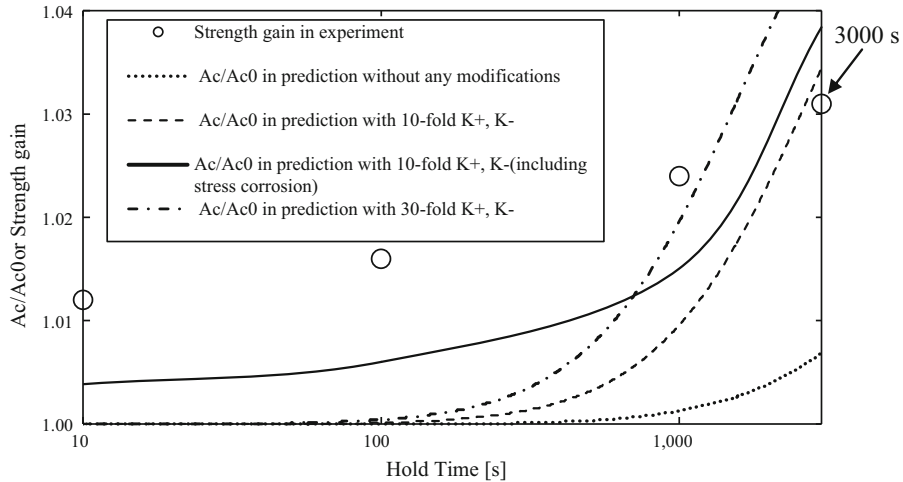


Figure 7

Comparison of predicted growth of contact area with strength evolution observed in the experiment. The prediction uses 1-fold, 10-fold, 10-fold (including stress corrosion) and 30-fold dissolution/precipitation rate constant,  $k_+/k_-$ . The experimental data for SHS test under 3 MPa effective normal stress

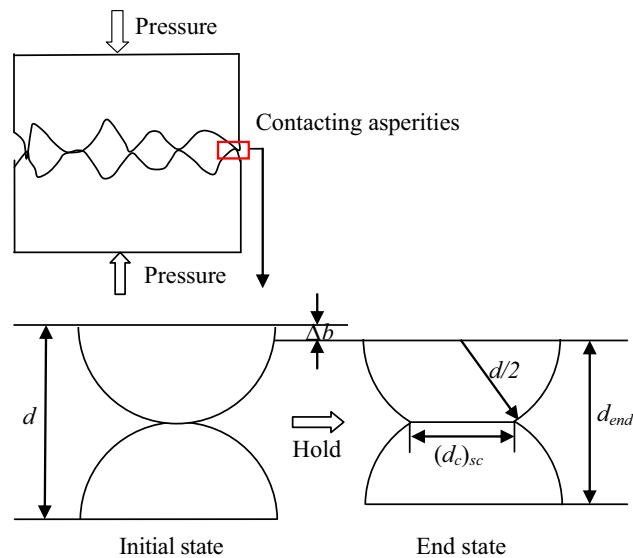


Figure 8

Schematic illustrations of compaction at grain-to-grain contacts during hold times. As the fracture closes, the contact area between contacting asperities (idealized as contacting spheres) increases

mechanistic model for pressure solution (YASUHARA *et al.* 2003, 2005) to represent the observed time-dependent increase in healing rate with hold time. However, this prediction fits only for long hold times ( $\sim 1000$  s) and returns large relative underestimations for short hold periods. This underestimation likely results since the model does not accommodate critical underlying mechanisms that operate at low stress, including the roles of cementation and stress corrosion. When the growth of contact area induced by stress corrosion is introduced into the mechanistic model, the predicted results better fit the experimental observations. Velocity-stepping tests show velocity strengthening (stable sliding) over shearing velocities range from 1 to 6  $\mu\text{m/s}$ . It is important to note that this velocity-strengthening response occurs within the experimental conditions in this work. Fluid-rock interactions also exert an influence on hydraulic properties of the fault structures and components. The observed permeability reduces throughout the experiment, indicating compaction of fracture aperture during sliding.

#### Acknowledgments

This work was funded by the special fund of the national '985' project of Zhejiang University. The

authors thank Steven L. Swavely and Hemant Kumar for their assistance in the laboratory experimentation.

#### REFERENCES

- ATKINSON K. (1979), *A fracture mechanics study of sub-critical tensile cracking of quartz in wet environments*, Pure Appl. Phys., 117, 1011–1024.
- BEELER, N. M., T. E. TULLIS, and J. D. WEEKS (1994), *The roles of time and displacement in the evolution effect on rock friction*, Geophys. Res. Lett., 21(18), 1987–1990, doi:10.1029/94GL01599.
- BOS, B., C. J. PEACH, and C. J. SPIERS (2000), *Slip behavior of simulated gouge-bearing faults under conditions favoring pressure solution*, J. Geophys. Res., 105, 16,699–16,717.
- BOS, B., and C. J. SPIERS (2002), *Fluid-assisted healing processes in gouge-bearing faults: Insights from experiments on a rock analogue system*, Pure Appl. Geophys., 159, 2537–2566.
- CARPENTER, B. M., D. M. SAFFER and C. MARONE (2012), *Frictional properties and sliding stability of the San Andreas fault from deep drill core*, Geology, 40(8), 759–762; doi:10.1130/G33007.1.
- CHESTER J.S., C. LENZ, F. M. CHESTER, and R. A. LANG (2004), *Mechanisms of compaction of quartz sand at diagenetic conditions*, Earth Planet. Sci. Lett., 220(3), 435–451.
- COLLETTINI, C., A. NIEMEIJER, C. VITI, and C. MARONE (2009a), *Fault zone fabric and fault weakness*, Nature, 462, 907–910, doi:10.1038/nature08585.
- COLLETTINI, C., C. VITI, S. A. F. SMITH, and R. E. HOLDSWORTH (2009b), *The development of interconnected talc networks and weakening of continental low-angle normal faults*, Geology, 37, 567–570, doi:10.1130/G25645A.1.

- CUBILLAS, P., M. PRIETO, S. KÖHLER, C. CHAÏRAT, and EH OELKERS (2005), *Experimental determination of the dissolution rates of calcite, aragonite, and bivalves*. Chem. Geol., 216 (1–2), 59–77. [10.1016/j.chemgeo.2004.11.009](https://doi.org/10.1016/j.chemgeo.2004.11.009).
- DEWERS T., A. HAJASH (1995), *Rate laws for water-assisted compaction and stress-induced water-rock interaction in sandstones*, J. Geophys. Res., 100, 13093–13112.
- DIETERICH, J. H. (1972), *Time-dependent friction in rocks*, J. Geophys. Res., 77, 3690–3697.
- DIETERICH, J. H. (1979), *Modeling of rock friction. 1. Experimental results and constitutive equations*, J. Geophys. Res. 84, 161–162,–168.
- DIETERICH, J. H. (1981), *Constitutive properties of faults with simulated gouge*, Geophys. Monogr. 24, 103–120.
- DIETERICH, J. H., and B. D. KILGORE (1994), *Direct observation of frictional contacts: New Insights for state-dependent properties*, Pure Appl. Geophys., 143, 283–302, doi:[10.1007/BF00874332](https://doi.org/10.1007/BF00874332).
- EVANS, J.P., F. M. CHESTER (1995), *Fluid-rock interaction in faults of the San Andreas system: Inferences from San Gabriel fault rock geochemistry and microstructures*, J. Geophys. Res., 100(B7), 13007–13020.
- GIGER, S. B., E. TENTHOREY, S. F. COX, and J. D. FITZ Gerald (2007), *Permeability evolution in quartz fault gouges under hydrothermal conditions*, J. Geophys. Res., 112, B07202, doi:[10.1029/2006JB004828](https://doi.org/10.1029/2006JB004828).
- GOREN, L., E. AHARONOV, D. SPARKS, R. TOUSSAINT (2010), *Pore pressure evolution in deforming granular material: A general formulation and the infinitely stiff approximation*. J. Geophys. Res., 115(9), B09216.
- GOREN, L., E. AHARONOV, D. SPARKS, R. TOUSSAINT (2011), *The mechanical coupling of fluid-filled granular material under shear*, Pure Appl. Geophys., 168(12), pp. 2289–2323.
- GRATIER, J-P., D. DYSTHE, F. RENARD (2013), *The role of pressure solution creep in the ductility of the Earth's upper crust*. Adv. Geophys., 54, doi: [10.1016/B978-0-12-380940-7.00002-0](https://doi.org/10.1016/B978-0-12-380940-7.00002-0).
- HICKMAN, S. H., and B. EVANS (1992), *Growth of grain contacts in halite by solution transfer: Implications for diagenesis, lithification and strength recovery*, in *Fault Mechanics and Transport Properties of Rocks*, pp. 253–260, Academic, London, doi:[10.1016/S0074-6142\(08\)62825-9](https://doi.org/10.1016/S0074-6142(08)62825-9).
- HICKMAN, S., R. SIBSON, and R. BRUHN (1995), *Introduction to special section: Mechanical involvement of fluids in faulting*, J. Geophys. Res., 100, 12,831–12,840.
- HIROSE, T. and T. SHIMAMOTO (2005), *Slip-weakening distance of faults during frictional melting as inferred from experimental and natural pseudotachylytes*, Bull. Seismol. Soc. Am., 95, 1666–1673.
- HOLDSWORTH, R. E. (2004), *Weak faults—Rotten cores*, Science, 303, 181–182, doi:[10.1126/science.1092491](https://doi.org/10.1126/science.1092491).
- IKARI, M. J., D. M. SAFFER, and C. MARONE (2007), *Effect of hydration state on the frictional properties of montmorillonite-based fault gouge*, J. Geophys. Res., 112, B06423, doi:[10.1029/2006JB004748](https://doi.org/10.1029/2006JB004748).
- IKARI, M. J., D. M. SAFFER, and C. MARONE (2009), *Frictional and hydrologic properties of clay-rich fault gouge*, J. Geophys. Res., 114, B05409, doi:[10.1029/2008JB006089](https://doi.org/10.1029/2008JB006089).
- IKARI, M. J., C. MARONE, and D. M. SAFFER (2011), *On the relation between fault strength and frictional stability*, Geology, 39, 83–86, doi:[10.1130/G31416.1](https://doi.org/10.1130/G31416.1).
- INSKEEP, W. P., and P. R. BLOOM (1985), *An evaluation of rate-equations for calcite precipitation kinetics at pCO2 less than 0.01 atm and pH greater than 8*. Geochim. Cosmochim. Acta, 49 (10), 2165–2180.
- JOHNSON T. (1981), *Time-dependent friction of granite: implications for precursory slip on faults*, J. Geophys. Res. 86, 6017–6028.
- KARNER, S. L., C. MARONE, and B. EVANS (1997), *Laboratory study of fault healing and lithification in simulated fault gouge under hydrothermal conditions*, Tectonophysics, 277, 41–55, doi:[10.1016/S0040-1951\(97\)00077-2](https://doi.org/10.1016/S0040-1951(97)00077-2).
- LI, Q., T. E. TULLIS, D. GOLDSBY, and R. W. CARPWICK (2011), *Frictional ageing from interfacial bonding and the origins of rate and state friction*, Nature, 480, 233–236, doi:[10.1038/nature10589](https://doi.org/10.1038/nature10589).
- MAIR, K., and C. J. MARONE (1999), *Friction of simulated fault gouge for a wide range of velocities and normal stresses*, J. Geophys. Res., 104, 28899–28914.
- MARONE, C. J. (1998), *Laboratory-derived friction laws and their application to seismic faulting*, Annu. Rev. Earth Planet. Sci., 26(1), 643–696.
- MARONE, C. J. (2004), *Earthquake science: faults greased at high speed*, Nature, 427, 405–406.
- MARONE C., C. H. SCHOLZ (1988), *The depth of seismic faulting and the upper transition from stable to unstable slip regimes*, Geophys. Res. Lett. 15, 621–624.
- MCGUIRE, T.P. (2012), *Permeability evolution of stressed fractures permeated by reactive fluids*, The Pennsylvania State University, State College, US.
- MCGUIRE, T. P., D. ELSWORTH, Z. KARZC (2013), *Experimental Measurements of Stress and Chemical Controls on the Evolution of Fracture Permeability*, Trans. Porous Med., 98, 15–34 DOI [10.1007/s11242-013-0123-4](https://doi.org/10.1007/s11242-013-0123-4).
- MIZOGUCHI, K., T. HIROSE, T. SHIMAMOTO, and E. FUKUYAMA (2006), *Moisture-related weakening and strengthening of a fault activated at seismic slip rates*, Geophys. Res. Lett., 33, L16319, doi: [10.1029/2006GL026980](https://doi.org/10.1029/2006GL026980).
- MIZOGUCHI, K., M. TAKAHASHI, K. MASUDA, and E. FUKUYAMA (2007), *Fault strength drop due to phase transitions in the pore fluid*, Geophys. Res. Lett., 34, L09313, doi:[10.1029/2007GL029345](https://doi.org/10.1029/2007GL029345).
- MOORE, D. E., and D. A. LOCKNER (2007), *Friction of the smectite clay montmorillonite. The Seismogenic Zone of Subduction Thrust Faults*, edited by T. Dixon and C. Moore, pp. 317–345, Columbia Univ. Press, New York.
- MUHURI, S. K., T. A. DEWERS, T. E. SCOTT Jr., and Z. RECHES (2003), *Interseismic fault strengthening and earthquake-slip instability: Friction or cohesion?*, Geology, 31, 881–884, doi:[10.1130/G19601.1](https://doi.org/10.1130/G19601.1).
- NAKASHIMA, S. (1995), *Diffusivity of ions in pore water as a quantitative basis for rock deformation rate estimates*, Tectonophysics, 245, 185–203.
- NARA Y., K. KANEKO (2005), *Study of subcritical crack growth in andesite using the double torsion test*, Int. J. Rock Mech. Min. Sci., 42: 521– 530.
- NIEMEIJER, A., C. MARONE, and D. ELSWORTH (2010a), *Fabric induced weakness of tectonic faults*, Geophysical Research Letters, 37, L03304, doi:[10.1029/2009GL041689](https://doi.org/10.1029/2009GL041689).
- NIEMEIJER, A. R., and R. L. VISSERS (2014), *Earthquake rupture propagation inferred from the spatial distribution of fault rock frictional properties*, Earth Planet. Sci. Lett., 396, 154–164.
- OLSEN, M. P., C. H. SCHOLZ, and A. LE GER (1998), *Healing and sealing of a simulated fault gouge under hydrothermal conditions: Implications for fault healing*. J. Geophys. Res., 103, 7421–7430.

- RABINOWICZ, E. (1951), *The nature of static and kinetic coefficients of friction*, J. Appl. Phys., 22, 1373–1379, doi:10.1063/1.1699869.
- RECHES, Z., and D. A. LOCKNER (2010), *Fault weakening and earthquake instability by powder lubrication*, Nature, 467(7314), 452–455, doi:10.1038/nature09348.
- RENARD, F., J.-P. GRATIER, and B. JAMTVEIT (2000), *Kinetics of crack-sealing, intergranular pressure solution, and compaction around active faults*, J. Struct. Geol., 22(10), 1395–1407.
- REVLIN, A. (1999), *Pervasive pressure-solution transfer: A poro-visco-plastic model*, Geophys. Res. Lett., 26(2), 255–258.
- ROBIN, F. (1978), *Pressure solution at grain-to-grain contacts*, Geochim. Cosmochim. Ac., 42: 1383–1389.
- SAFFER, D. M., and C. MARONE (2003), *Comparison of smectite- and illite-rich gouge frictional properties: Application to the updip limit of the seismogenic zone along subduction mega-thrusts*, Earth Planet. Sci. Lett., 215, 219–235, doi:10.1016/S0012-821X(03)00424-2.
- SCHOLZ, C. H. (1998), *Earthquakes and friction laws*. Nature, 391, 37–42.
- SCHOLZ, C. H. (2002), *The Mechanics of Earthquakes and Faulting*, 2nd ed., Cambridge Univ. Press, Cambridge, U. K., doi:10.1017/CBO9780511818516.
- TENTHOREY, E., S. F. COX, and H. F. TODD (2003), *Evolution of strength recovery and permeability during fluid-rock reaction in experimental fault zones*, Earth Planet. Sci. Lett., 206, 161–172.
- VERBERNE, B. A., C. HE, and C. J. SPIERS (2010), *Frictional properties of sedimentary rocks and natural fault gouge from the Longmen Shan fault zone, Sichuan, China*, Bull. Seismol. Soc. Am., 100(5B), 2767–2790.
- VIOLAY, M., S. NIENSEN, E. SPAGNUOLO, D. CINTI, G. DI TORO, G. DI STEFANO (2013), *Pore fluid in experimental calcite-bearing faults: Abrupt weakening and geochemical signature of co-seismic processes*, Earth Planet. Sci. Lett., 361, pp. 74–84.
- VIOLAY, M., S. B. NIENSEN, B. GIBERT, E. SPAGNUOLO, A. CAVALLO, P. AZAIS, S. VINCIGUERRA, G. DI TORO (2014), *Effect of water on the frictional behavior of cohesive rocks during earthquakes*. Geology, 42(1), pp. 27–30.
- VOLERY, C., E. DAVAUD, C. DURLET, B. CLAVEL, J. CHAROLLAIS, AND B. CALINE (2010), *Microporous and tight limestones in the Urgonian Formation (late Hauterivian to early Aptian) of the French Jura Mountains: Focus on the factors controlling the formation of microporous facies*, Sediment. Geol., 230(1), 21–34, doi:10.1016/j.sedgeo.2010.06.017.
- WINTSCH, R. P., R. CHRISTOFFERSEN, and A. K. KRONENBERG (1995), *Fluid-rock reaction weakening of fault zones*, J. Geophys. Res., 100, 13,021–13,032, doi:10.1029/94JB02622.
- YASUHARA, H., C. MARONE, and D. ELSWORTH (2005), *Fault zone restrengthening and frictional healing: The role of pressure solution*, J. Geophys. Res., 110, B06310, doi:10.1029/2004JB003327.
- YASUHARA, H., and D. ELSWORTH (2008), *Compaction of a fracture moderated by competing roles of stress corrosion and pressure solution*, Pure Appl. Geophys., 165, 1289–1306, doi:10.1007/s00024-008-0356-2.
- YASUHARA, H., D. ELSWORTH, and A. POLAK (2003), *A mechanistic model for compaction of granular aggregates moderated by pressure solution*, J. Geophys. Res., 108(B11), 2530, doi:10.1029/2003JB002536.
- YASUHARA, H., D. ELSWORTH, and A. POLAK (2004), *Evolution of permeability in a natural fracture: Significant role of pressure solution*, J. Geophys. Res., 109(B3), B03204.
- YASUHARA, H., D. ELSWORTH, A. POLAK, J. LIU, A. GRADER, and P. HALLECK (2006), *Spontaneous switching between permeability enhancement and degradation in fractures in carbonate: Lumped parameter representation of mechanically- and chemically-mediated dissolution*, Transp. Porous Med., 65(3), 385–409.
- ZHANG, X., C. J. SPIERS, and C. J. PEACH (2010), *Compaction creep of wet granular calcite by pressure solution at 28°C to 150°C*, J. Geophys. Res., 115, B09217, doi:10.1029/2008JB005853.

(Received December 29, 2014, revised April 13, 2015, accepted April 23, 2015)